Distributed and localized feedback in microresonator sequences for linear and nonlinear optics

John E. Heebner

Institute of Optics, University of Rochester, Rochester, New York 14627

Philip Chak

Department of Physics, University of Toronto, Toronto, Ontario M5S 1A7, Canada

Suresh Pereira

Institut für Theorie der Kondensierten Materie, Universität Karlsruhe, Germany

John E. Sipe

Department of Physics, University of Toronto, Toronto, Ontario M5S 1A7, Canada

Robert W. Boyd

Institute of Optics, University of Rochester, Rochester, New York 14627

Received November 3, 2003; revised manuscript received April 4, 2004; accepted May 19, 2004

Sequences of optical microresonators can be used to construct densely integrated structures that display slow group velocity, ultrahigh or low dispersion of controllable sign, enhanced self-phase modulation, and nonlinear optical switching. We consider four archetypal geometries consisting of effectively one-dimensional sequences of coupled microresonators. Two of these cases exhibit distributed feedback such as is found in a traditional multilayered structure supporting photonic bandgaps. The other two exhibit localized feedback and resonant enhancement but are free from photonic bandgaps. All of these structures offer unique properties useful for controlling the propagation of light pulses on a chip. © 2004 Optical Society of America

OCIS codes: 230.5750, 190.4390, 190.4360, 190.5530, 130.3120, 250.5300.

1. INTRODUCTION

The strengths of dispersion and optical nonlinearity are two key parameters that control the length scale over which pulses evolve, acquire phase, or perform switching operations in a photonic medium.[1] It has been argued that of all photonic devices, microresonators currently provide the highest dispersion per unit volume.[2] Microresonators also effectively increase interaction lengths and produce increased circulating intensities.[3–5] These two ingredients, when combined, can dramatically enhance nonlinear optical properties. As a consequence of their compact geometry and tailorable dispersive and nonlinear optical properties, microresonators are expected to play a key role in the large-scale integration of photonic devices.

In this paper, we compare and contrast the light-propagation characteristics associated with different connection geometries for sequences of microring (or whispering-gallery microdisk) resonators. We restrict our attention to four archetypal building blocks from which sequences can be constructed. For each of these four ring-based units, a direct analog in the form of a traditional Fabry–Perot cavity is depicted in Fig. 1. With the insight provided by these Fabry–Perot analogs, it is clear that these geometries identify the four ways of connecting four-port resonators[6] to form sequences.

A sequence based on Fig. 1(a), (cavity version) represents the traditional multilayered structure or Bragg grating. The ring-based version of such a multilayer is a sequence of directly coupled rings, often termed a coupled-resonator optical waveguide[7,8] (CROW). Another way to couple the rings is indirectly through a common waveguide, as depicted in Fig. 1(b). Such is the case in a side-coupled integrated spaced sequence of resonators, or SCISSOR.[9] The other two ways [(c) and (d)] are characterized by indirect coupling of rings via *two* common waveguides. Note that these four structures are identical in terms of their fundamental building block and differ only in the manner in which they are interconnected. Of the cavity versions, only geometry (a) forms a building block that is naturally sequenced as in a multilayered structure. The other three geometries possess interchanged ports that do not sequence naturally in their cavity embodiments and can be constructed only with greater complexity. Ring resonators are, however,

0740-3224/2004/101818-15$15.00

more naturally suited to sequencing in *any* of these geometries because the two input and two output ports occupy spatially distinct channels. Furthermore, their planar nature is compatible with current fabrication technologies.[10–12] We expect that it is generally not appreciated that coupled microring resonator structures offer three more possible configurations, and it is hoped that this paper will help elucidate the fundamental features and differences associated with the propagation of light in each of these photonic microstructures.

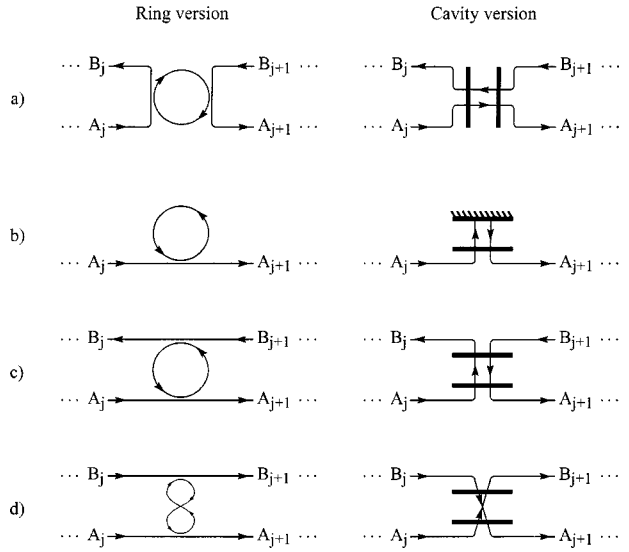

Fig. 1. Illustrations of four archetypal ring-resonator unit cells for (a) a CROW, (b) a single-channel SCISSOR, (c) a double-channel SCISSOR, and (d) a twisted double-channel SCISSOR, along with their cavity versions. These unit cells can serve as building blocks for constructing sequences of resonators that serve as novel photonic guidance architectures.

2. RESONATOR FUNDAMENTALS

We first review the basic properties of coupled ring resonators. Resonance frequencies occur at $\nu_m = mc/2\pi nR$, where the resonance order m is an integer, and it is assumed that the refractive index n and radius R are effective values for the circulating mode in the resonator.

For the sake of simplicity, we parameterize the coupling strengths by lumped self-coupling r and cross-coupling t coefficients. These symbols are deliberately chosen analogously to the field reflection and transmission coefficients associated with cavity mirrors or dielectric interfaces. The resulting resonances are often characterized by a finesse parameter, $\mathcal{F}$, which depends on these coupling strengths.[13] The finesse provides a convenient estimate of the effective number of round trips light makes through the resonator and of the peak of the intensity buildup of light, defined as the ratio of the intensity in the ring to the input intensity.

In Fig. 2, we compare the transmission characteristics of single- and double-coupled ring resonators. A single-

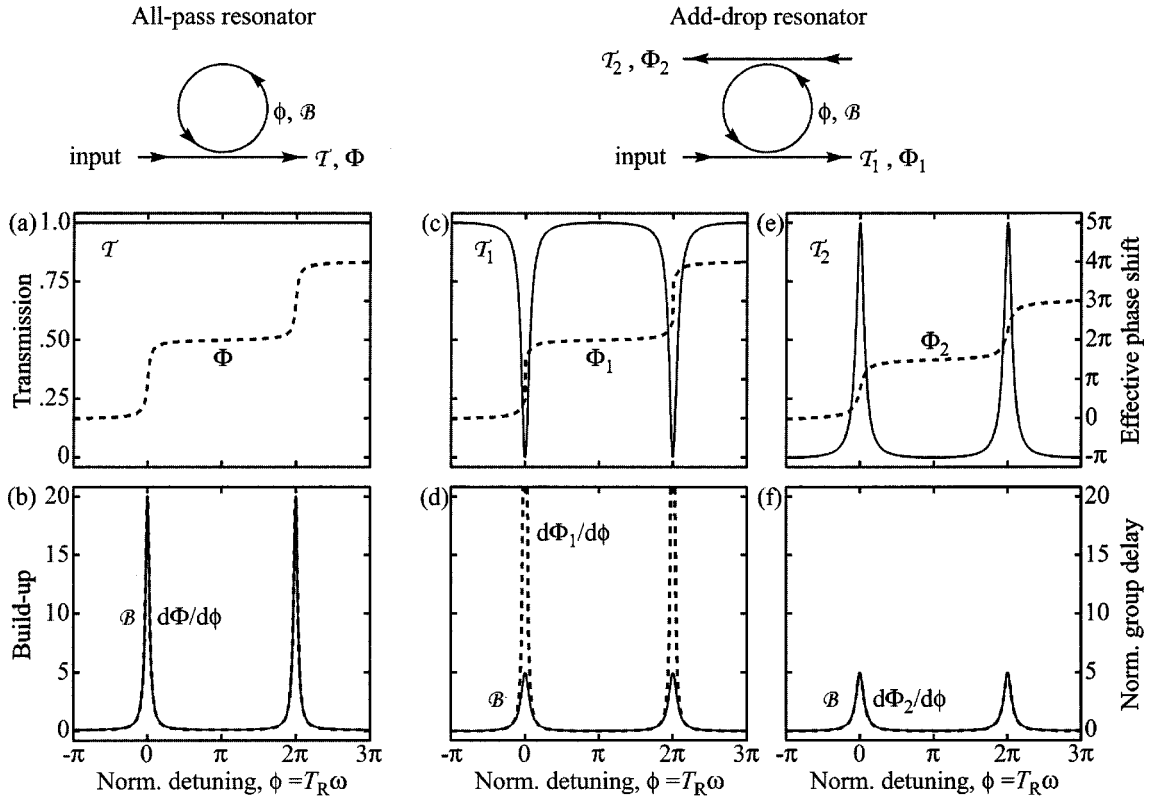

Fig. 2. Amplitude transmission (solid curves) and effective phase shift (dashed curves) for (a) an all-pass resonator, (c) through port of an add-drop resonator, and (e) drop port of an add–drop resonator. Plots (b), (d), and (f) display the coherent intensity buildup (solid curves) and group delay normalized with respect to single-pass transit time (dashed curves) for the same ports as in (a), (c), and (e), respectively. The independent variable on all plots is the normalized detuning (radian frequency multiplied by ring transit time), and all coupling coefficients are $t^2 = 0.1814$.

coupled ring resonator behaves like a Gires–Tournois resonator (a Fabry–Perot resonator with a 100% reflecting back interface). Provided that the internal losses are negligible, all frequencies are passed with unit transmission, and the device is termed an all-pass filter.[14] Spectral components in the vicinity of a resonance spend more time circulating in the resonator, or more precisely, experience a larger group delay. Figure 2(a) shows the (flat) transmission and effective phase shift Φ, due to passage through the resonator plotted against normalized frequency $\phi = \omega T_R$, where the normalizing parameter is the ring transit time, $T_R = 2\pi nR/c$. The coherent buildup of intensity $\mathcal{B}$ and the normalized group delay in units of the ring transit time, $d\Phi/d\phi$, are shown in Fig. 2(b). Note that both are equally enhanced near a resonance.

The addition of a second waveguide qualitatively changes the behavior of the device. Functionally, it has found use as an add–drop filter[15] such that spectral components near resonances are diverted to one (drop) port, while the rest pass to another (through) port. Spectral components near a resonance can be introduced to the through port by means of the remaining (add) port. Figures 2(c) and 2(e) show the amplitude and phase of the transmission function at each of the output ports. The coherent buildup of intensity in the resonator and the group delay for each port are shown in Figs. 2(d) and 2(f). In the case of balanced couplers, the peak buildup is 1/4 times as large as that attained in an all-pass resonator for the same coupling strength. The peak group delay at the drop port is also reduced by 1/4, while the resonant group delay at the through port diverges at the point of zero transmission.

The field of optical filter synthesis has adopted these two basic ring resonators as fundamental amplitude- and phase-filtering elements.[16,17] In the next section, we develop a formalism that extends these concepts to sequences.

3. BLOCH-MATRIX FORMALISM

We now describe a simple matrix-based technique that can generate the linear spectral properties of a single resonator as well as that of an infinite sequence of coupled resonators. The fields at a single coupling point as depicted in Fig. 3 are related by the real self- and cross-coupling parameters, r and t, according to

$$E_3 = rE_1 + itE_2,$$

$$E_4 = itE_1 + rE_2.$$

Neglecting loss allows the simple relation $r^2 + t^2 = 1$ to hold for each coupler. Using these relations for each coupling point as required, we can calculate the matrix M that relates the fields at the two right ports of a coupled resonator, A_{j+1} and B_{j+1}, to the fields at the two left ports A_j and B_j. For a generic four-port optical device, this takes the form

$$\begin{pmatrix} A_{j+1} \\ B_{j+1} \end{pmatrix} = \begin{bmatrix} M_{11} & M_{12} \\ M_{21} & M_{22} \end{bmatrix} \begin{pmatrix} A_j \\ B_j \end{pmatrix}, \tag{1}$$

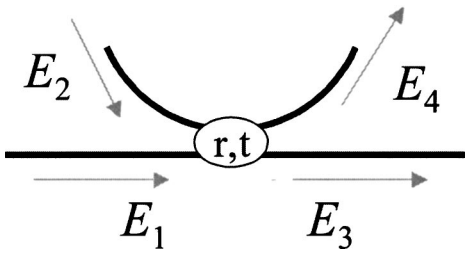

Fig. 3. Schematic depicting the fields associated with a resonator-to-waveguide coupling point. The field amplitudes across the coupling point are related by the self- and cross-coupling coefficients (r and t) as described in the text.

and in Table 1, we show the components M_{ij} that represent the port-to-port relations associated with each of the building blocks in Fig. 1.

We are now ready to consider an infinite sequence of resonators, each of the same building block and connected to its neighbors, with spatial periodicity L. Bloch's theorem states that we can find solutions for the fields that at periodic intervals in the infinite lattice are simply related by a phase factor:

$$\begin{pmatrix} A_{j+1} \\ B_{j+1} \end{pmatrix} = \exp(ik_{\text{eff}}L) \begin{pmatrix} A_j \\ B_j \end{pmatrix}. \tag{2}$$

That is, $\exp(ik_{\text{eff}}L)$ must be an eigenvalue of the matrix formed from M_{ij}; for this to hold, we require

$$\det \begin{bmatrix} M_{11} - \exp(ik_{\text{eff}}L) & M_{12} \\ M_{21} & M_{22} - \exp(ik_{\text{eff}}L) \end{bmatrix} = 0. \tag{3}$$

The quadratic formula is applied to the expanded form of this equation to obtain the dispersion relation (ω versus k_{eff}) based on the matrix coefficients that in general are frequency dependent:

$$\exp(i2k_{\text{eff}}L) - (M_{11} + M_{22})\exp(ik_{\text{eff}}L) + (M_{11}M_{22} - M_{12}M_{21}) = 0, \tag{4}$$

$$k_{\text{eff}} = \frac{1}{L}\arg\left[\frac{(M_{11} + M_{22})}{2} \pm \left(\frac{(M_{11} - M_{22})^2}{4} + M_{12}M_{21}\right)^{1/2}\right]. \tag{5}$$

In the following sections, we apply this technique to derive dispersion relations for the four archetypal infinite periodic lattices that result from connecting the unit cells in Fig. 1.

4. DIRECTLY COUPLED RESONATORS

A sequence of directly coupled resonators[18] with no auxiliary waveguides is depicted in Fig. 4. One interpretation of this geometry results from considering every other resonator to act as two auxiliary waveguides that connect the unit cells of Fig. 1(a) together in sequence. Consequently, the optical properties are analogous to the familiar multilayered Bragg stack.

In order to allow for a richness of greater complexity, we consider a structure with two length scales where the resonator circumference alternates between $2\pi R_1$ and $2\pi R_2$. In what follows, we will restrict ourselves to the case where light propagates clockwise in the larger reso-

Table 1. Matrix Elements M_{ij}, for the Four Coupled Microresonator Unit Cells Shown in Fig. 1[a]

Structure	M_{11}	M_{12}	M_{21}	M_{22}
(a) CROW	$\dfrac{-\exp\left[i\dfrac{(\phi_2+\phi_1)}{2}\right]+r^2\exp\left[-i\dfrac{(\phi_2-\phi_1)}{2}\right]}{t^2}$	$\dfrac{r}{t^2}\left[\exp\left(i\dfrac{\phi_2}{2}\right)-\exp\left(-i\dfrac{\phi_2}{2}\right)\right]$	M_{12}^*	M_{11}^*
(b) One-channel SCISSOR	$\dfrac{[1-r\exp(-i\phi)]\exp(i\theta)}{r-\exp(-i\phi)}$	0	0	0
(c) Two-channel SCISSOR	$\dfrac{[1-r_1r_2\exp(-i\phi)]\exp(i\theta)}{r_1-r_2\exp(-i\phi)}$	$\dfrac{-t_1t_2\exp\left(i\dfrac{\phi}{2}\right)}{r_2-r_1\exp(i\phi)}$	$\dfrac{-t_1t_2\exp\left(-i\dfrac{\phi}{2}\right)}{r_1-r_2\exp(-i\phi)}$	$\dfrac{[1-r_1r_2\exp(i\phi)]\exp(-i\theta)}{r_2-r_1\exp(i\phi)}$
(d) Twisted SCISSOR	$\dfrac{[r_1-r_2\exp(i\phi)]\exp(i\theta)}{1-r_1r_2\exp(i\phi)}$	$\dfrac{-t_1t_2\exp\left(i\dfrac{\phi}{2}\right)\exp(i\theta)}{1-r_1r_2\exp(i\phi)}$	$\dfrac{-t_1t_2\exp\left(i\dfrac{\phi}{2}\right)\exp(i\theta)}{1-r_1r_2\exp(i\phi)}$	$\dfrac{[r_2-r_1\exp(i\phi)]\exp(i\theta)}{1-r_1r_2\exp(i\phi)}$

[a] Here $\phi = 2\pi Rn\omega/c$ and $\theta = Ln\omega/c$.

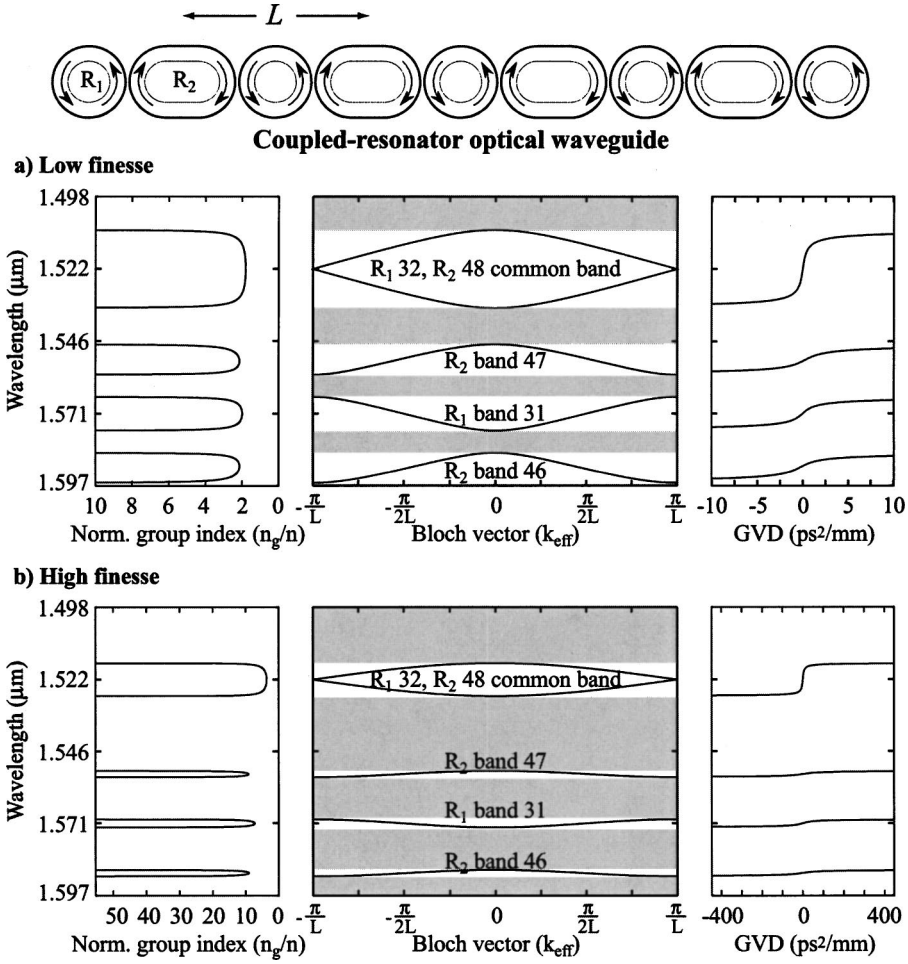

Fig. 4. Dispersion relation, normalized group index, and GVD for (a) a low-finesse and (b) a high-finesse coupled-resonator optical waveguide. The dispersion relation is analogous to that of a multilayered structure with alternating layer indices and/or thicknesses. Bandgaps are always of the direct type and result from distributed Bragg reflection. Parameters include a refractive index of $n = 3.1$, alternating radii of $R_1 = 2.5\ \mu$m, and $R_2 = 1.5R_1$. Resonances $m_{R1} = 31$ and 32 and $m_{R2} = 46$, 47, and 48 are shown. In (a), a high coupling strength, $t^2 = 0.75$, results in narrow bandgaps, while in (b), a low coupling strength, $t^2 = 0.1814$, results in wide bandgaps. These qualitative features are directly opposite those found in the double-channel SCISSOR.

nators and counterclockwise in the smaller resonators. Implementing Eq. (5) and Table 1 entry (a), the dispersion relation for an infinite sequence is given by

$$k_{\mathrm{eff}} = \frac{-i}{2(R_1 + R_2)} \arg\left(\left[\frac{-1}{t^2} \cos\left(\frac{\phi_1 + \phi_2}{2} \right) + \frac{r}{t^2} \cos\left(\frac{\phi_2 - \phi_1}{2} \right) \right] \pm \left\{ \left[\frac{-1}{t^2} \cos\left(\frac{\phi_1 + \phi_2}{2} \right) + \frac{r}{t^2} \cos\left(\frac{\phi_2 - \phi_1}{2} \right) \right]^2 - 1 \right\}^{1/2} \right), \tag{6}$$

where the two phase degrees of freedom, $\phi_j = 2\pi R_j n \omega / c$, are proportional to the two characteristic length scales. The two solutions represent the forward- and backward-going waves throughout the structure. As a consequence of *distributed feedback*, photonic bandgaps emerge where the Bragg condition is satisfied [$2\pi R_j = (m + 1/2)\lambda/n$]. The dispersion relation, normalized group index [$(c/n)\mathrm{d}k_{\mathrm{eff}}/\mathrm{d}\omega$], and group-velocity dispersion (GVD) ($\mathrm{d}^2 k_{\mathrm{eff}}/\mathrm{d}\omega^2$) are plotted in Fig. 4 for a sequence of resonators at wavelengths near 1.55 μm. The shaded areas represent bandgaps, while the bands are labeled according to the nearest resonance order (m). The structure may be used to support Bragg soliton propagation,[19] particularly near the band edges where the group-velocity dispersion is strong[20] and the nonlinearity is enhanced.

5. SINGLE-CHANNEL SCISSORS

A single-channel SCISSOR as depicted in Fig. 5 is composed of a sequence of all-pass resonators as in Fig. 1(b). Because no mechanism for contradirectional coupling is present, light of all frequencies is simply transmitted in a feed-forward sequential manner from resonator to resonator "pausing" for *localized feedback* at each. As a result, no photonic bandgaps can exist in this geometry. The optical properties are in fact independent of whether or not

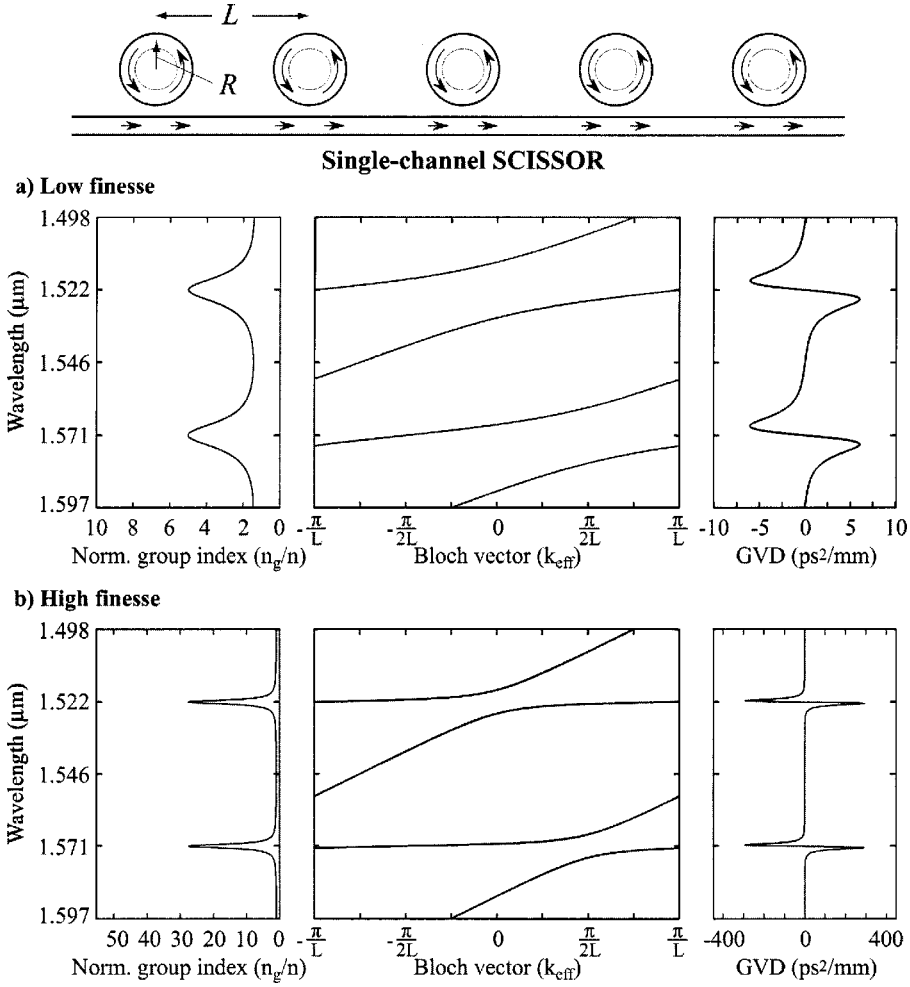

Fig. 5. Dispersion relation, normalized group index, and GVD for (a) a low-finesse and (b) a high-finesse single-channel SCISSOR. Note that the dispersion relation does not display photonic bandgaps. Nevertheless, at the resonances ($\lambda_m = 2\pi n R/m$), the group index (and the intensity buildup) is maximized. Parameters include a refractive index of $n = 3.1$ and a radius of $R = 2.5$ μm. Resonances $m_R = 31$ and 32 at 1.571 μm and 1.522 μm are shown. In (a), a high coupling strength, $t^2 = 0.75$, results in a wide bandwidth, while in (b), a low coupling strength, $t^2 = 0.1814$, results in a narrow bandwidth. To avoid redundancy, and because the forward- and backward-traveling waves do not couple, only the dispersion relation for the forward-traveling wave is shown.

all the spacings between neighboring resonators are the same; only the average density of resonators in a given length (or simply the total number) dictates the optical properties of the structure. For an infinite periodic SCISSOR, the only surviving matrix coefficient is M_{11} (see Table 1).

The dispersion relation (5) takes the form

$$k_{\text{eff}} = \frac{n}{c}\omega + \frac{1}{L}\arg\left[\frac{r - \exp(i\phi)}{1 - r\exp(i\phi)}\right] = \frac{n}{c}\omega + \frac{\Phi(\omega)}{L}, \tag{7}$$

where $\phi = 2\pi R n\omega/c$, and $\Phi(\omega)$ is the accumulated phase shift of a single resonator [see Fig. 2(a)]. The dispersion relation, normalized group index, and GVD are plotted in Fig. 5 for a series of 2.5-μm radius resonators at wavelengths near 1.55 μm. To avoid confusion, the dispersion relation is shown only for forward-going propagation, defined by the arrows in the schematic. For resonance frequencies, light experiences group delays of the order of the cavity lifetime $(2\mathcal{F}/\pi)2\pi nR/c$ at each resonator. From a macroscopic point of view, the discrete delays may be considered to be distributed along the channel resulting in an effective group velocity that can be slower than that in the common waveguide. On resonance, the group index scales directly with finesse as $n_g = [1 + (4R/L)\mathcal{F}]n$ for $r \approx 1$. As a consequence of the frequency-dependent nature of the effective group velocity, which peaks at resonance, the lowest-order dispersion vanishes on resonance but can be very strongly normal (positive) or anomalous (negative) below or above each resonance, respectively. Furthermore, because light pulses effectively traverse each resonator many times and the circulating intensity in the resonators is coherently increased, the accumulation of nonlinear phase shift or self-phase modulation[21] is enhanced in quadratic proportion to the finesse.[5] This fact suggests that high values of finesse need not be required to see strong nonlinear effects. In a previous paper, it was demonstrated that the propagation of pulse envelopes through such a structure can be accurately modeled with a reduced wave equation such as the nonlinear Schrödinger equation.[22] SCISSOR soliton formation, modulation instability, self-steepening, pulse compression, and many other effects resulting from an interaction between nonlinearity and dispersion traditionally require large pulse energies and/or kilometers of interaction length in optical fiber. However, these effects can be observed with modest pulse energies and a *six* order-of-magnitude reduction in length scale with SCISSORs. Other coupled-cavity structures have been shown to enhance nonlinearities[23] and support soliton propagation.[24] The SCISSOR structure is interesting in its ability to slow, disperse, and/or intensify light pulses while maintaining a transmission spectrum free from bandgaps—a feature which, to the best of our knowledge, does not bear direct analogy with *any* traditional artificial medium. Fundamentally, this results from disabling distributed feedback throughout the structure and localizing it to the all-pass resonators.

6. DOUBLE-CHANNEL SCISSORS

The addition of a second common coupling channel to a SCISSOR as depicted in Fig. 6 enables distributed feedback. The unit cell for this structure is an add–drop resonator oriented as in Fig. 1(c). In contrast to the single-channel case, the spacing between resonators is now important because resonances can develop not only within the resonators but also among them. Photonic bandgaps emerge around each type of resonance in the dispersion relation of an infinite periodic structure. One type of bandgap emerges when the periodicity of the structure satisfies the Bragg condition ($2L = m_B\lambda/n$, with m_B an integer), and another type emerges when the circumference of the microresonator is an integer multiple of the wavelength ($2\pi R = m_R\lambda/n$, with m_R an integer). Compared with a multilayered structure or CROW, the output port connections (drop and through) at each unit cell are reversed. This reversal couples what were distributed Bragg reflections to the feed-forward direction and diverts resonance frequencies to the retroreflected direction. In the case of a multilayered structure or CROW, high reflectivity can be achieved by distributed feedback from many partially reflecting unit cells, and 100% transmission is always obtained at a resonant frequency. In contrast, in a double-channel SCISSOR, 100% reflection is readily achieved at any of the resonator's resonant frequencies irrespective of the coupling parameter r, provided that the coupling coefficients are matched. This result is attributed to the well-known phenomena of critical coupling, whereby incident light is completely attenuated at the resonance frequency owing to complete destructive interference of the bypassed incoming field with the out-coupled circulating field. For this condition to be met, the sum of the tap coupling due to the second channel (and losses if present in the ring) must equal the cross coupling from the excitation channel.

Implementing Eq. (5), the dispersion relation for the double-channel SCISSOR structure takes the form

$$\begin{aligned} k_{\text{eff}} = \frac{1}{L}\arg\Bigg(&\frac{1}{2}\frac{1 - r_1 r_2\exp(-i\phi)}{r_1 - r_2\exp(-i\phi)}\exp(i\theta) \\ &+ \frac{1}{2}\frac{1 - r_1 r_2\exp(i\phi)}{r_2 - r_1\exp(i\phi)}\exp(-i\theta) \\ &\pm \Bigg\{\Bigg[\frac{1}{2}\frac{1 - r_1 r_2\exp(-i\phi)}{r_1 - r_2\exp(-i\phi)}\exp(i\theta) \\ &- \frac{1}{2}\frac{1 - r_1 r_2\exp(i\phi)}{r_2 - r_1\exp(i\phi)}\exp(-i\theta)\Bigg]^2 \\ &+ \frac{(1 - r_1^2)(1 - r_2^2)}{[r_2 - r_1\exp(i\phi)][r_1 - r_2\exp(-i\phi)]}\Bigg\}^{1/2}\Bigg), \end{aligned} \tag{8}$$

where the two phase degrees of freedom, $\phi = 2\pi R n\omega/c$ and $\theta = L n\omega/c$, are proportional to the two characteristic length scales. The two solutions represent the bottom-channel forward- and top-channel backward-going waves in the photonic structure. The dispersion relation, group index, and GVD are plotted in Fig. 6 for 2.5-μm-radius resonators spaced by $1.5\pi R$ at wavelengths near 1.55 μm.

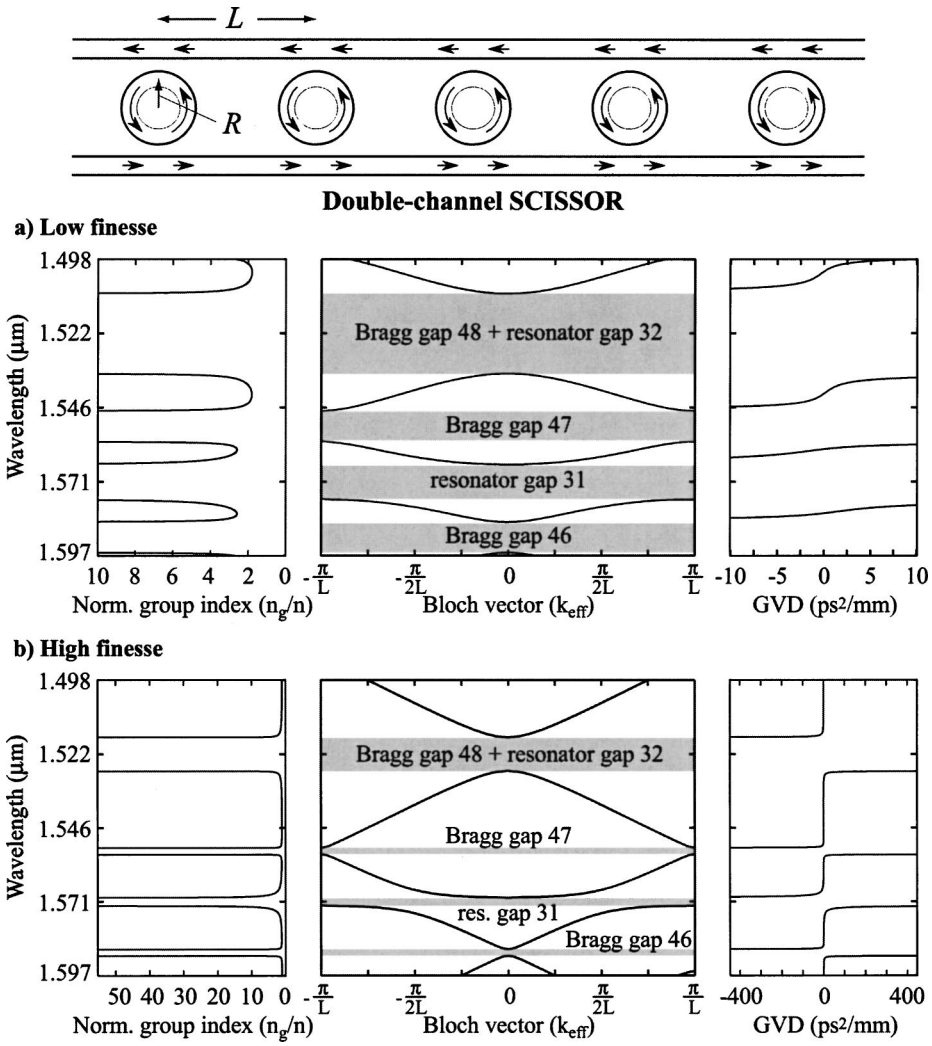

Fig. 6. Dispersion relation, normalized group index, and GVD for (a) a low-finesse and (b) high-finesse double-channel SCISSOR. Note that unlike the dispersion relation for the single-guide SCISSOR, the double-guide variety displays photonic bandgaps. Two qualitatively different bandgaps manifest themselves. For spectral components satisfying the Bragg condition ($\lambda_{m_B} = 2nL/m_B$), the bandgap is direct and results from distributed Bragg reflection. At the resonances of the rings ($\lambda_{m_R} = 2\pi nR/m_R$), the bandgap is indirect and results from strong resonator-mediated backcoupling. Parameters were chosen such that one Bragg gap was coincident with one resonator gap within the figure: refractive index $n = 3.1$, radii $R = 2.5\ \mu$m, and spacing $L = 1.5\pi R$. Resonator resonances $m_R = 31$ and 32 and Bragg resonances $m_B = 46$, 47 and 48 are shown. The coincident resonator ($m_R = 32$) and Bragg ($m_B = 48$) resonance results in a wide direct gap. In (a), a high coupling strength, $t^2 = 0.75$, results in wide bandgaps, while in (b), a low coupling strength, $t^2 = 0.1814$, results in narrow bandgaps.

Of the two types of gaps mentioned above, those associated with the periodicity of the structure (interresonator spacing) are called "Bragg gaps" and are always direct. The indirect gaps are termed "resonator gaps" and are those associated with the internal resonances of the resonators. A comparison of the qualitative features of the dispersion relation reveals that the bandgaps are wider for low-finesse resonators. The interpretation is simple: In the high-finesse case, the band over which the individual resonators are *reflecting* is narrow, while in the low-finesse case it is wide. This directly carries over to the widths of the bandgaps in the infinitely periodic structure and is in stark contrast to the situation of a multilayered structure where high reflectivity results in a wider bandgap. As a consequence of the efficient excitation of the resonators near stop gaps, this structure is ideal for exploring nonlinear effects *within the bandgap*, such as gap solitons.[25,26]

7. TWISTED DOUBLE-CHANNEL SCISSORS

A "twist" on the double-channel SCISSOR, which possesses qualitatively different optical properties, is constructed by interchanging the top ports (add and drop) of each unit cell, as in Fig. 1(d). For optical fiber ring resonators, this configuration may be implemented by twisting each of the resonators to form figure-8 loops. In an integrated geometry, it is easier to build two resonators that are nearly 100% coupled. This "twisted" double-channel SCISSOR is depicted in Fig. 7. As a result of the port interchange, there is no longer any mechanism for contradirectional coupling, but codirectional coupling

across the channels is now mediated by the resonators with localized feedback enhancement. Thus light injected into one of the ports only couples to either of the channels in the forward-going direction. The structure therefore behaves as a resonator-enhanced directional coupler. In Table 1, the matrix coefficients are given taking the coefficients characterizing the couplings between the waveguides and resonators to be r_1 and r_2, and assuming that the twisted structure is implemented by use of two resonators that are 100% coupled to each other.

For an infinite periodic structure, the resulting dispersion relation (5) is

$$k_{\text{eff}} = \frac{1}{L}\arg\left[\exp(i\theta) + \frac{\left[\dfrac{r_1 - r_2\exp(i\phi)}{1 - r_1 r_2\exp(i\phi)} + \dfrac{r_2 - r_1\exp(i\phi)}{1 - r_1 r_2\exp(i\phi)}\right]}{2} \pm \left(\frac{\{[r_1 - r_2\exp(i\phi)] - [r_2 - r_1\exp(i\phi)]\}^2 + 4(1 - r_1^2)(1 - r_2^2)\exp(i\phi)}{4[1 - r_1 r_2\exp(i\phi)]^2}\right)^{1/2}\right], \quad (9)$$

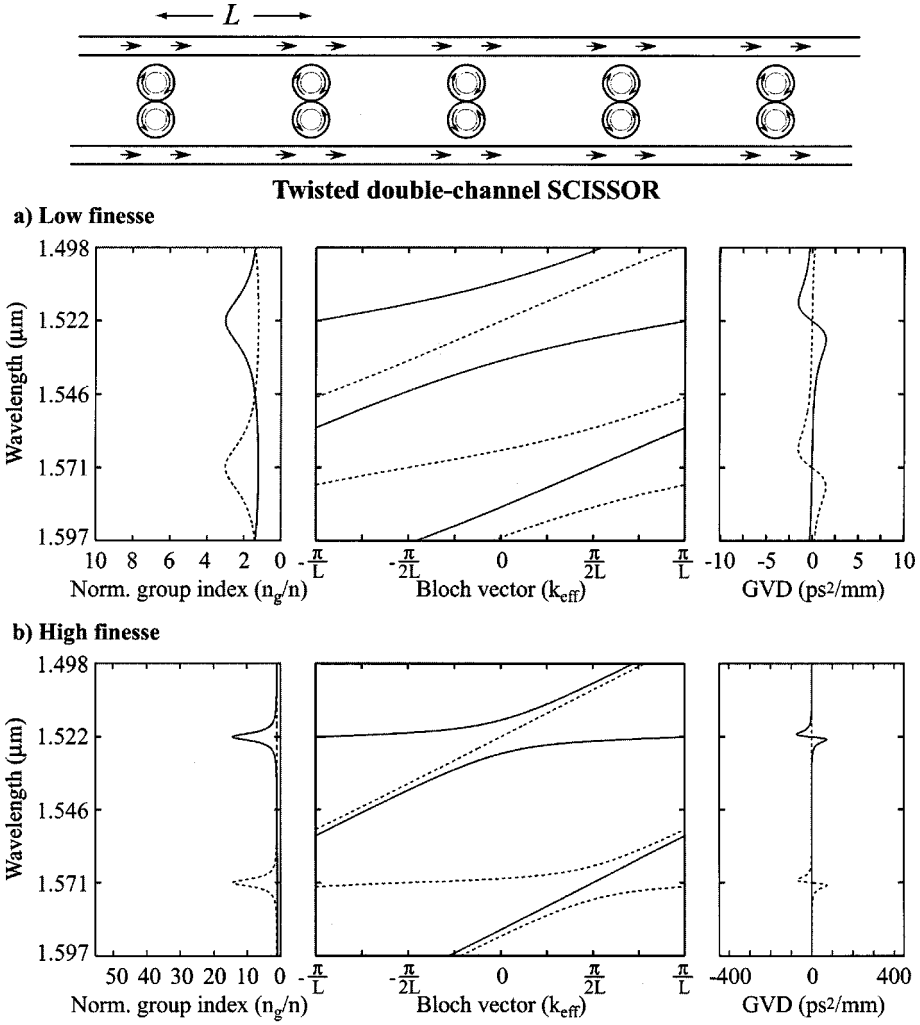

Fig. 7. Dispersion relation, normalized group index, and GVD for (a) a low-finesse and (b) a high-finesse twisted double-channel SCISSOR. Bandgaps are absent in the dispersion relation, which resembles that of the single-channel SCISSOR, but with the presence of a second branch. The two branches correspond to the two decoupled forward-traveling normal modes. Near the ring resonances ($\lambda_m = 2\pi nR/m$), the two branches are strongly coupled, as in the case of a directional coupler. Parameters used are the same as in Fig. 6 except that there are two resonators, each half in circumference and 100% coupled. Resonances $m_R = 31$ and 32 at 1.571 μm and 1.522 μm are shown. In (a), a high coupling strength, $t^2 = 0.75$, results in wide-bandwidth channel-to-channel coupling, while in (b) a low coupling strength, $t^2 = 0.1814$, results in narrow-bandwidth channel-to-channel coupling. To avoid redundancy, and because the two forward- and two backward-traveling waves do not couple, only the two forward-traveling dispersion relation branches are shown.

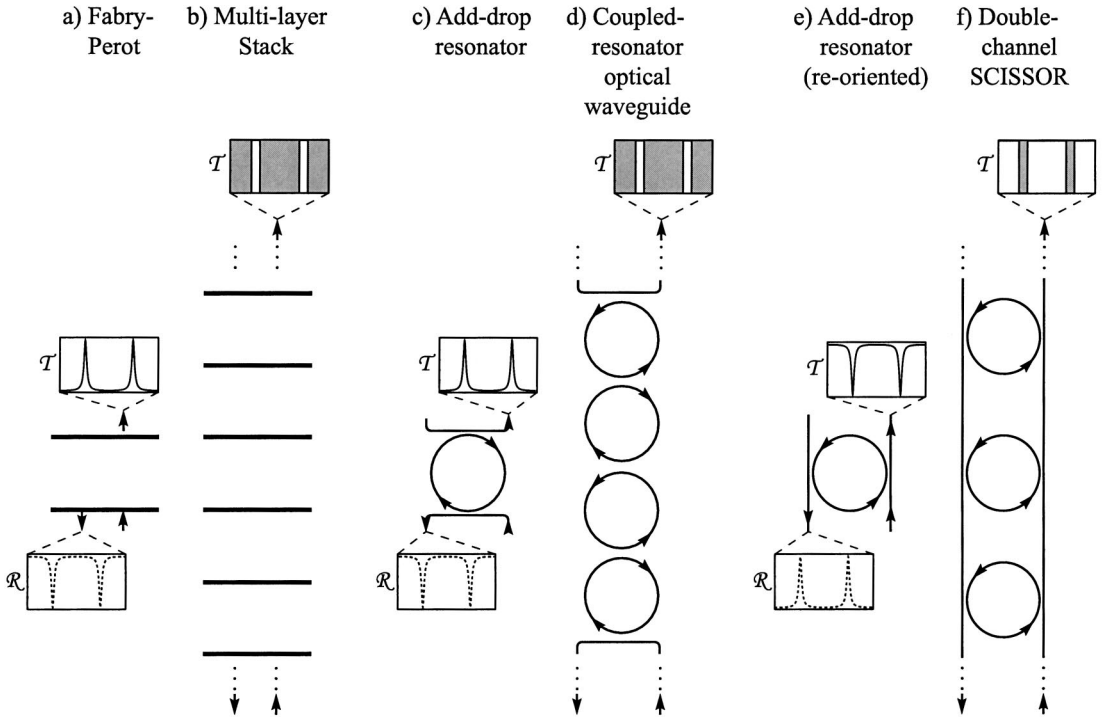

Fig. 8. Qualitative comparison of the transmission properties of three structures possessing bandgaps: (a) a Fabry-Perot, (b) a multilayered stack, (c) an add–drop resonator, (d) a CROW, (e) a double-channel resonator, and (f) an add–drop resonator (reoriented). Note that the qualitative features of the transmission peaks and valleys are equivalent for multilayered stacks and CROWs but reversed for double-channel SCISSORs. With increasing finesse, the bandgap widths increase in both multilayered stacks and CROWs, while they decrease in double-channel SCISSORs.

where $\phi = 2\pi Rn\omega/c$ and $\theta = Ln\omega/c$. The solutions represent the two coupled forward-going waves in the photonic structure. The dispersion relation, normalized group index, and GVD are plotted in Fig. 7 for the symmetric case of $r_1 = r_2$. Two branches are present, each one corresponding to one of two normal modes of the structure.

8. BANDGAP ENGINEERING IN DISTRIBUTED-FEEDBACK STRUCTURES

Figure 8 qualitatively compares the transmission properties of unit structures and infinite periodic structures for a double-guide SCISSOR and a multilayered structure. While a multilayered structure or CROW allows propagation on resonance and takes advantage of maximum coherent buildup of intensity within the resonators, propagation is not allowed at resonances of the double-channel SCISSOR around which bandgaps form.

We next compare the qualitative features of the transmission for a finite double-channel SCISSOR and CROW with the corresponding infinite periodic structures. The finite structures are termed parallel and serial resonator-coupled structures, respectively, in the literature.[27–31] Figure 9 displays the transmission spectra for *low-finesse* 1, 5, and infinite unit-celled structures. Figure 10 displays the transmission spectra for equivalent *high-finesse* structures. The displayed plots show that the dispersion relation can provide a heuristic guide to the location and width of the transmission dips in a finite structure. It is evident that the infinite double-channel SCISSOR and

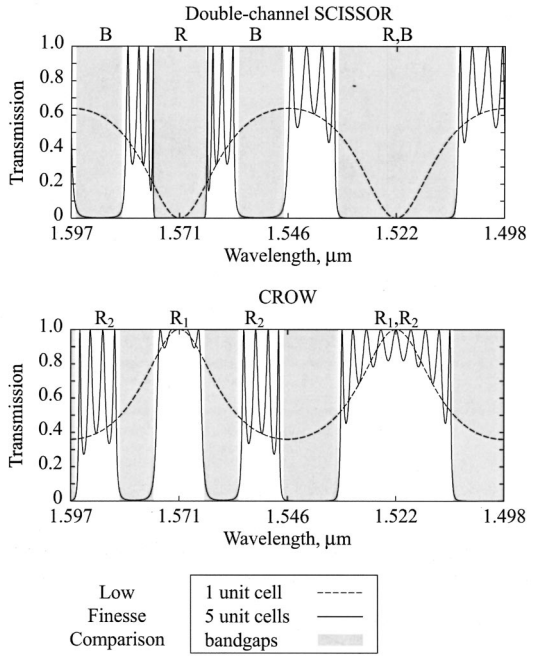

Fig. 9. Transmission spectra for a *low-finesse* ($t^2 = 0.75$) finite double-channel SCISSOR and finite CROW. Parameters are the same as in Figs. 4 and 6. Here, five unit cells are used to approximate the structures. For comparison, the transmission for a single resonator is shown in each case, and shaded regions correspond to one-dimensional photonic bandgaps in the corresponding infinite structure. The labels B and R correspond to the double-channel SCISSOR's Bragg and resonator gaps, while the labels R_1 and R_2 correspond to the alternating CROW resonances.

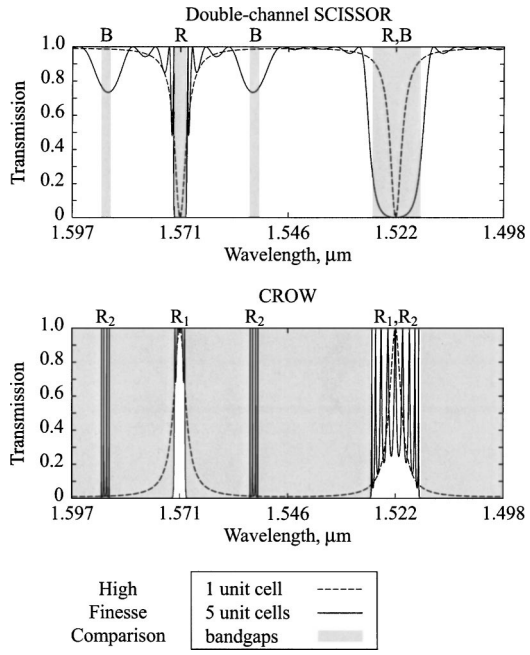

Fig. 10. Transmission spectra for a *high-finesse* ($t^2 = 0.1814$) finite double-channel SCISSOR and finite one-dimensional CROW. Parameters are the same as in Figs. 4 and 6. Here, five unit cells are used to approximate the structures. For comparison, the transmission for a single resonator is shown in each case, and shaded regions correspond to one-dimensional photonic bandgaps in the corresponding infinite structure. The labels B and R correspond to the double-channel SCISSOR's Bragg and resonator gaps, while the labels R_1 and R_2 correspond to the alternating CROW resonances.

CROW possess complementary transmission characteristics; that is, band and bandgap locations are interchanged. Typically, waveguide or fiber Bragg gratings possess low reflectivity (and thus low finesse) per unit cell, resulting in small ripples in the passbands. Here, the deep ripples in the transmission bands result from the abruptly terminated ends of the structure as encountered in unapodized high-reflectivity multilayered stacks. First, note that the ripple depth across the passbands is controlled by the transmission of a single resonator and results from the "splitting" of individual interacting resonances. Second, note that in going from low to high finesse, the widths of the single-resonator transmission dips (and peaks) shrink faster than the corresponding gaps (and bands) in the infinite structure. Analysis of the bandwidths show that, while the single resonator dip (and peak) bandwidth scales as $\mathcal{F}^{-1} \approx t^2/\pi$, the widths of infinite resonator gaps (and bands) scale as $\mathcal{F}_\infty^{-1} \approx 2t/\pi \propto \sqrt{\mathcal{F}^{-1}}$. This explains why the passband ripples are of similar depth in the low-finesse cases while are strong only in the high-finesse case for the CROW.

9. SLOW-LIGHT AND GROUP-VELOCITY DISPERSION

The dispersion relations associated with the microresonator-based photonic structures considered in this paper reveal greatly reduced group velocities ($v_g = \mathrm{d}\omega/\mathrm{d}k_{\mathrm{eff}}$) near structural resonances.[32] The reduction of group velocity may be intuitively understood by noting that near a structural resonance light spends extra time circulating localized within the resonators or in propagating back and forth between distributed components of the periodic structure. There are several criteria by which one can compare different optical mechanisms that induce slow-light effects. Furthermore, different applications demand different criteria. For some applications, the slowest attainable group velocity may be desirable. Many optical systems have demonstrated such slow-light capability[33] but typically only over bandwidths that are too narrow for practical use in optical communications or logic. For such applications, a large *fractional* group delay $(L/\tau)\mathrm{d}k_{\mathrm{eff}}/\mathrm{d}\omega$ is a better measure. This dimensionless quantity is interpreted as the number of pulse widths τ by which a pulse or train of pulses can be delayed, while still maintaining the integrity of the pulses. Many instances of slow-light phenomena, while impressive in their ability to slow the speed of pulse propagation to a small fraction of c, would fail to delay an incoming pulse by more than a fraction of a pulse width without seriously distorting it, simply because of a large accompanying group-velocity dispersion or narrow spectral window.

Microresonator-based structures have been proposed[34] for use as optical delay lines because, when designed properly, they can exhibit a large fractional delay. Additionally, because the group velocity can be made tunable by shifting resonances thermally[35] or electrically,[36] controllable optical delay lines can be constructed. The shortest pulse for which the group delay is meaningful, and thus that for which the fractional delay is largest, is one with a pulse width that matches the cavity lifetime. Shorter pulses become distorted as a consequence of high-order dispersive effects, while longer pulses, which experience the same physical delay, exhibit a lower fractional delay.

These considerations remind us that a vanishingly small group velocity is often not the sole important feature. An optical delay line or buffer based on microresonator structures will in general be useful only if slow group velocity is accompanied by high transmission and low pulse-distorting dispersion. Near resonances of a single-channel SCISSOR, the fractional group delay can approach unity. The single-channel SCISSOR exhibits maximum pulse delay on resonance with a wide open transmission window, albeit with nonnegligible third-order dispersion. In an earlier publication,[37] it was shown that in sacrificing some slowness by detuning above resonance and implementing self-phase modulation to balance the group velocity dispersion, third-order dispersion may be eliminated, and slow solitons may be propagated with high fidelity limited by residual fourth-order dispersion. In distributed-feedback structures, the edges of two bandgaps can be engineered so that they are close in frequency but not overlapping, resulting in a flat, defect like band generated between them.

Alternatively, the strong group-velocity dispersion encountered at certain frequencies can be put to use for the construction of photonic devices that perform dispersion compensation in an ultracompact geometry. Each of the structures in this paper can display group-velocity dispersion values that greatly exceed 20 ps^2 per millimeter.

These are at least 6 orders of magnitude higher than what is conventionally measured in typical single-mode silica fiber (20 ps^2 per kilometer). The situation is similar to that encountered in photonic crystal defect guides, which exhibit ultrastrong dispersive effects.[38] Just as an intrinsically high group-velocity reduction is not as important in many applications as a large fractional group delay, many photonics applications require strong fractional group-delay dispersion irrespective of the actual group-velocity dispersion. Microresonator-based structures have been implemented as dispersion compensators[39] because, when designed properly, can exhibit a fractional group-delay dispersion near unity (of either sign) per resonator. Additionally, the soliton period for a SCISSOR soliton is governed by the dispersion strength and dictates the length scale over which soliton pulse evolution can take place.

10. ENHANCED SELF-PHASE MODULATION WITH LOCALIZED FEEDBACK

Nonlinear effects in microresonators have been studied experimentally both in lasers and switching devices.[40–47] Coupled microresonator structures have been shown to possess propagation characteristics associated with extended nonlinear Schrödinger equations. The phenomena of slow light, light trapping,[48] soliton propagation,[9] soliton compression,[22] soliton switching,[49] gap solitons,[26] self-steepening, modulation instability, and four-wave mixing are all directly transferrable to the much more compact scale afforded by a microresonator-based photonic structures.

The enhancement of nonlinear effects in microresonators is attributed to two different though related effects. First, because the group velocity is reduced in such a way that light circulates through a longer path length within a photonic structure, the interaction length (or time) for a nonlinear process is increased. This is directly related to the well-known enhancement of phase sensitivity in ring-resonator,[5] multilayered,[50] and photonic crystal-based[51] structures. Second, because the light circulating within the resonators is coherently builtup to a higher intensity than that which is initially injected into the structure, stronger nonlinear effects are possible. As a result of these two effects, nonlinear processes like self-phase modulation are enhanced in proportion to the square of the resonator finesse.[5] This scaling law holds for single resonators and localized-feedback structures. For example, in the case of the single-channel SCISSOR, the phase sensitivity and buildup are coincident and equal, and the enhancement of accumulated nonlinear phase shifts is directly proportional to the square of the group index, $(c/v_g)^2$. This is a general result that is typically found in many nonlinear photonic systems displaying slow-light effects resulting from structural resonances. The finesse provides a good estimate of the scaling of nonlinear effects, even if the losses due to scattering and absorption that we have neglected in this paper are taken into account. For example, linear attenuation and group delay, which are length dependent but not intensity dependent, are each increased in linear proportion to the finesse. Nonlinear phase shifts, which depend on the intensity-length product, are increased in quadratic proportion to the finesse. But the efficiency of some nonlinear frequency-conversion processes can be enhanced in even greater proportions.[52]

We next examine the trade-off between bandwidth and nonlinear strength for enhanced self-phase modulation in a single-channel SCISSOR. The bandwidth of a resonator is primarily governed by its radius and finesse,

$$\Delta\nu = c/(2\pi R n \mathcal{F}). \tag{10}$$

For a single add–drop filter, this bandwidth corresponds to the width of the narrow-band add or drop transmission windows. For a single all-pass filter, this bandwidth corresponds to the frequency interval over which the phase varies sensitively and in a nearly linear manner over π radians. Outside this interval, the sensitivity falls and the phase significantly departs from linear behavior such that a pulse with a larger bandwidth can become severely distorted by higher-order dispersive terms. There is an exact trade-off for linear properties. A resonator's lifetime, group delay, and interaction length may be increased at the expense of bandwidth in direct proportion to the finesse. Such trade-offs can be fortuitously circumvented for certain nonlinear properties. The strength of the enhanced self-phase modulation may be characterized by how much power is required to achieve a nonlinear phase shift of π radians in a structure composed of a few resonators. To good approximation, the threshold power required to achieve a π nonlinear phase shift in just a single all-pass resonator is given by

$$P_\pi \approx \frac{\lambda A_{\text{eff}}}{4\mathcal{F}^2 n_2 R}. \tag{11}$$

The ratio of the reduced threshold power to the reduced bandwidth for a resonator of a given finesse is a form of figure of merit and is related to the threshold pulse energy. The minimum pulse energy required to achieve the π nonlinear phase shift is obtained when the pulse width is of the order of the inverse of the resonator bandwidth. This is easily understood because a longer pulse with the same peak power will carry more energy but not be any more effective at accumulating nonlinear phase. A

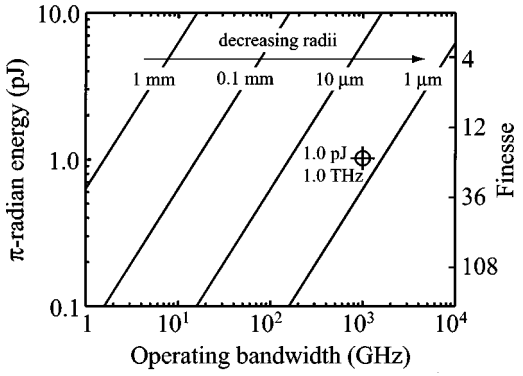

Fig. 11. Inherent trade-off between bandwidth and energy required to achieve a π nonlinear phase shift *per resonator* in a single-channel SCISSOR structure. The diagonal lines correspond to constant resonator diameter for AlGaAs or chalcogenide-based systems near 1.55 μm. Increasing finesse is directly proportional to decreasing energy.

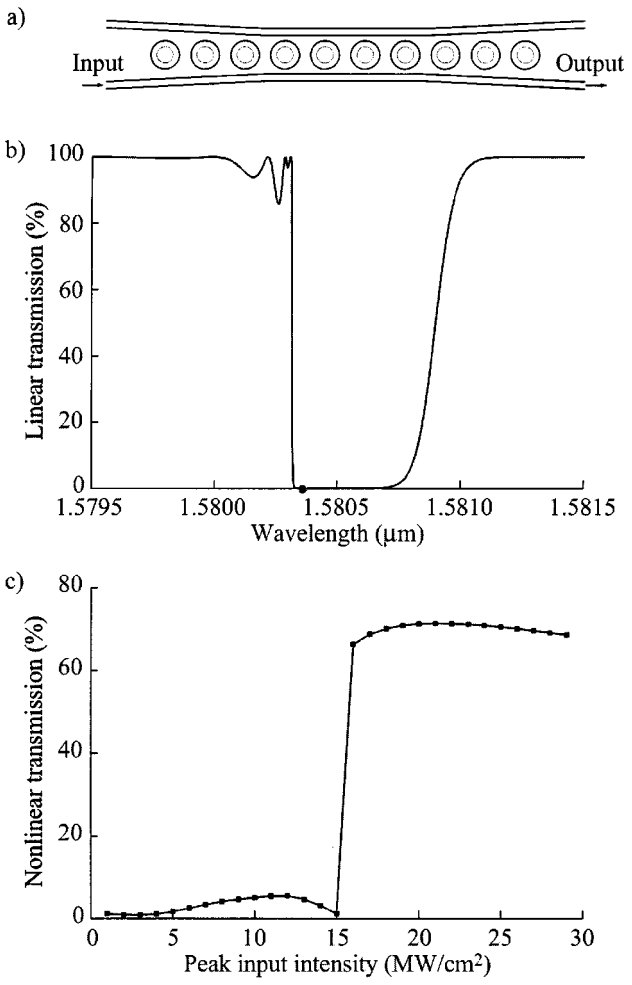

Fig. 12. Nonlinear pulse simulation assuming a Kerr nonlinearity in a double-channel SCISSOR structure with ten unit cells. A schematic of the structure is shown in (a). A 100-ps Gaussian (FWHM) pulse is injected into the two-channel structure at the input port (lower channel). Parameters include a refractive index of 3.1, radii of $R = 4.1$ μm, and spacing $L = 16$ μm. The apodization profile is discussed in the text. The carrier wavelength of the pulse is at $\lambda = 1.58$ μm, which is close to the 51st resonance of the resonator. A plot of the linear transmission spectrum of the structure is displayed in (b). The carrier wavelength of the input pulse is indicated by a black dot in the figure. A plot of the transmission versus peak input intensity for the Gaussian pulse is displayed in (c). Notice that the switching threshold is at approximately 15 MW/cm^2 and may be obtained with picosecond pulses with energies less than 0.15 pJ when the effective areas of the guides are less than one square micron.

shorter pulse will not allow the resonator sufficient time to buildup in intensity and thus will experience a weakened nonlinear response in addition to being severely distorted. For a high-contrast dielectric waveguide, the effective area to which the power is confined may be as small as $\lambda^2/8n^2$, where n is the refractive index of the guiding layer. The threshold energy required to achieve a π nonlinear phase shift is accordingly reduced in linear proportion to finesse:

$$\mathcal{E}_\pi = \frac{\lambda^3 \sqrt{\pi \ln(2)}}{16 \mathcal{F} n n_2 c}. \tag{12}$$

In order to reduce the parameter space, we make some practical choices ($n = 3, n_2 = 1.5 \times 10^{-17}$ m^2/W) corresponding to AlGaAs[53,54] or chalcogenide[55–57] glass waveguides operating near 1.55 μm. Figure 11 displays the trade-off between the energy requirement for a π-radian nonlinear phase shift per resonator and bandwidth for resonators of varying diameter. It is of technological interest to note that a π nonlinear phase shift is obtainable with a 1-picosecond, 1-picojoule pulse by use of a single ultracompact microresonator of moderate finesse.

11. NONLINEAR OPTICAL SWITCHING

To demonstrate the nonlinear effect in a microresonator structure that exhibits bandgaps, we consider nonlinear switching in a double-channel SCISSOR structure. The numerical technique employed here is similar to that found in previous work.[22,52,58] The ten-celled two-channel structure that we consider is shown in Fig. 12(a). To improve the transmission spectrum of the structure, we apodized the cross-coupling coefficient of the structure using a linear apodization profile. The middle four cells were characterized by $r = 0.98$, while the first and the last three cells of the structure were apodized, according to $r = 0.995, 0.99, 0.985$. The resulting (linear) transmission spectrum is shown in Fig. 12(b). At the input port, a 100-ps pulse centered at the wavelength $\lambda = 1.58$ μm is injected into the structure. A plot of the transmission versus peak input intensity of the pulse is shown in Fig. 12(c). It is apparent that the transmission rises abruptly when the peak input intensity is higher than a certain threshold. The abrupt change in transmission near the threshold suggests that the structure is potentially useful as a switching device.[59]

12. PRACTICAL ISSUES

In practice, it is currently difficult to fabricate high-dielectric contrast ring and disk resonators with low loss. Losses are high primarily due to scattering at rough edges.[60] Microsphere-based resonators have displayed ultrahigh quality factors and finesse values[61–67] but are difficult to integrate and make reproducibly. It has been shown that, for a given fixed figure of merit in a lossy nonlinear medium, significant improvement can be made over an ordinary straight channel by forming the channel into a resonator.[68] The introduction of loss into the structures considered in this paper reduces transmission and circulating intensity buildups while broadening resonances. The phase sensitivity, however, often increases with additional loss. As a result, the enhancement of nonlinear phase shift, which is proportional to phase sensitivity and buildup, is interestingly somewhat insensitive to loss. Transmission, of course, ultimately suffers with too much loss.

The photonic structures analyzed thus far in this paper have involved lossless infinite periodic structures. In practice, finite structures consisting of one or many unit cells may be implemented to achieve close approximations to these transfer characteristics. The number of interacting resonators will be limited by losses, reproducibility, and intrinsic dispersion of effective refractive

index of all guiding structures. Ultimately, the higher the intrinsic finesse (*unloaded*, before coupling), the better the fabricated resonators will perform as desired. Being able to accomplish useful tasks with low *loaded* finesse relaxes tolerances on the design and fabrication of multiple interacting resonators that require $\lambda/n\mathcal{F}$ precision. Fortunately, while low-finesse devices do not make good high-resolution add–drop filters or sensors, they can still possess strong nonlinear effects owing to the scaling laws presented.

13. SUMMARY

Microresonators confine light to circulate within and among compact photonic structures. Fabrication technology has advanced such that high-bandwidth microresonators are readily constructed from either high dielectric contrast "photonic wires"[69] or photonic crystals[70] for the enhancement of nonlinearities.[71,72] Both guiding structures have the ability to confine light to small dimensions and rely on large dielectric contrasts. The use of artificial media composed of sequences of microresonators is a promising approach to the construction of photonic waveguides with engineerable optical properties. Their exotic linear properties result from structural resonances that increase effective path lengths in a detuning-dependent manner. These linear properties can and have been exploited to build tunable optical delay lines, filters, and dispersion compensators. Their exotic nonlinear properties result from a combination of increased effective path lengths and coherent intensity buildup. These nonlinear properties can be exploited to construct optical switches, optical limiters, pulse compressors, pulse imagers,[73] and other nonlinear photonic devices relying on interplay with group-velocity dispersion. We expect microresonator-based structures to become essential components for integrated linear and nonlinear photonic applications.

ACKNOWLEDGMENTS

This work was sponsored by the Defense Advanced Research Projects Agency under grant MDA972-00-1-0021, the State of New York NYSTAR program as part of the Alliance for Nanomedical Technologies, the Natural Sciences and Engineering Research Council of Canada (NSERC), and Photonics Research Ontario. P. Chak acknowledges support from an Ontario Graduate Scholarship. We thank Q-Han Park, Nick Lepeshkin, Aaron Schweinsberg, and Richart Slusher for stimulating discussions. J. Heebner's present address is Lawrence Livermore National Laboratory, L-464, 7000 East Avenue, Livermore, California 94550.

REFERENCES AND NOTES

1. G. P. Agrawal, *Nonlinear Fiber Optics*, 3rd ed. (Academic, Calif., 2001).
2. B. E. Little and S. T. Chu, "Toward very large-scale integrated photonics," Opt. Photonics News **11**(11), 24–29 (2000).
3. G. I. Stegeman and C. Seaton, "Nonlinear integrated optics," J. Appl. Phys. **58**, 57 (1985).
4. V. B. Braginsky, M. L. Gorodetsky, and V. S. Ilchenko, "Quality-factor and nonlinear properties of optical whispering-gallery modes," Phys. Lett. A **137**, 393–397 (1989).
5. J. E. Heebner and R. W. Boyd, "Enhanced all-optical switching by use of a nonlinear fiber ring resonator," Opt. Lett. **24**, 847–849 (1999).
6. Strictly speaking, the first configuration is constructed from two-port resonators and is a special case.
7. A. Yariv, Y. Xu, R. K. Lee, and A. Scherer, "Coupled resonator optical waveguide: a proposal and analysis," Opt. Lett. **24**, 711–713 (1999).
8. Y. Xu, R. K. Lee, and A. Yariv, "Scattering theory analysis of waveguide-resonator coupling," Phys. Rev. E **62**, 7389–7404 (2000).
9. J. E. Heebner, R. W. Boyd, and Q. Park, "Slow light, induced dispersion, enhanced nonlinearity, and optical solitons in a resonator-array waveguide," Phys. Rev. E **65**, 036619 (2002).
10. D. Rafizadeh, J. P. Zhang, S. C. Hagness, A. Taflove, K. A. Stair, S. T. Ho, and R. C. Tiberio, "Waveguide-coupled AlGaAs/GaAs microcavity ring and disk resonators with high finesse and 21.6-nm free-spectral range," Opt. Lett. **22**, 1244–1246 (1997).
11. K. Djordjev, S. Choi, and P. D. Dapkus, "High-Q vertically coupled InP microdisk resonators," IEEE Photon. Technol. Lett. **14**, 331–333 (2002).
12. P. Michler, A. Kiraz, C. Becher, W. V. Schoenfeld, P. M. Petroff, L. Zhang, E. Hu, and A. Imamoglu, "A quantum dot single-photon turnstile device," Science **290**, 2282–2285 (2000).
13. We define the finesse as the free spectral range (FSR) divided by the full width at half-depth (FWHD) of the resonance peak. Applying this definition to either the normalized group delay or the intensity buildup of an all-pass resonator, the finesse is calculated as
$$\mathcal{F} = \frac{\mathrm{FSR}}{\mathrm{FWHD}} = \frac{2\pi}{2\arccos\left(\frac{2r}{1+r^2}\right)} \xrightarrow[r\approx 1]{} \frac{\pi}{1-r}.$$
In the case of the add–drop resonator, r is replaced with $r_1 r_2$.
14. C. K. Madsen and G. Lenz, "Optical all-pass filters for phase response design with applications for dispersion compensation," IEEE Photon. Technol. Lett. **10**, 994–996 (1998).
15. B. E. Little, S. T. Chu, H. A. Haus, J. Foresi, and J.-P. Laine, "Microring resonator channel dropping filters," J. Lightwave Technol. **15**, 998–1005 (1997).
16. B. E. Little, S. T. Chu, J. V. Hryniewicz, and P. P. Absil, "Filter synthesis for periodically coupled microring resonators," Opt. Lett. **25**, 344–346 (2000).
17. C. K. Madsen, "Efficient architectures for exactly realizing optical filters with optimum bandpass designs," IEEE Photon. Technol. Lett. **10**, 1136–1138 (1998).
18. R. Orta, P. Savi, R. Tascone, and D. Trinchero, "Synthesis of multiple ring resonator filters for optical systems," IEEE Photon. Technol. Lett. **7**, 1447–1449 (1995).
19. B. J. Eggleton, R. E. Slusher, C. M. de Sterke, P. A. Krug, and J. E. Sipe, "Bragg grating solitons," Phys. Rev. Lett. **76**, 1627–1630 (1996).
20. S. Mookherjea, D. S. Cohen, and A. Yariv, "Nonlinear dispersion in a coupled-resonator optical waveguide," Opt. Lett. **27**, 933–935 (2002).
21. R. W. Boyd, *Nonlinear Optics*, 2nd ed. (Academic, San Diego, Calif., 2003).
22. J. E. Heebner, R. W. Boyd, and Q. Park, "SCISSOR solitons and other propagation effects in microresonator modified waveguides," J. Opt. Soc. Am. B **19**, 722–731 (2002).
23. Y. Xu, R. K. Lee, and A. Yariv, "Propagation and second-harmonic generation of electromagnetic waves in a coupled-resonator optical waveguide," J. Opt. Soc. Am. B **17**, 387–400 (2000).
24. D. N. Christodoulides and N. K. Efremidis, "Discrete tem-

poral solitons along a chain of nonlinear coupled microcavities embedded in photonic crystals," Opt. Lett. **27**, 568–570 (2002).
25. W. Chen and D. L. Mills, "Gap solitons and the nonlinear optical response of superlattices," Phys. Rev. Lett. **58**, 160–163 (1987).
26. S. Pereira, J. E. Sipe, J. E. Heebner, and R. W. Boyd, "Gap solitons in a two-channel SCISSOR structure," Opt. Lett. **27**, 536–538 (2002).
27. S. T. Chu, B. E. Little, W. Pan, T. Kaneko, and Y. Kokubun, "Second-order filter response from parallel coupled glass microring resonators," IEEE Photon. Technol. Lett. **11**, 1426–1428 (1999).
28. J. V. Hryniewicz, P. P. Absil, B. E. Little, R. A. Wilson, and P.-T. Ho, "Higher order filter response in coupled microring resonators," IEEE Photon. Technol. Lett. **12**, 320–322 (2000).
29. G. Griffel, "Synthesis of optical filters using ring resonator arrays," IEEE Photon. Technol. Lett. **12**, 810–812 (2000).
30. A. Melloni, "Synthesis of a parallel-coupled ring-resonator filter," Opt. Lett. **26**, 917–919 (2001).
31. R. Grover, V. Van, T. A. Ibrahim, P. P. Absil, L. C. Calhoun, F. G. Johnson, J. V. Hryniewicz, and P.-T. Ho, "Parallel-cascaded semiconductor microring resonators for high-order and wide-FSR Filters," J. Lightwave Technol. **20**, 900–905 (2002).
32. A. Melloni, F. Morichetti, and M. Martinelli, "Optical slow wave structures," Opt. Photon. News **14**, 44–48 (2003).
33. R. W. Boyd and D. J. Gauthier, "Slow and fast light," Prog. Opt. **33**, 497–530 (2002).
34. G. Lenz, B. J. Eggleton, C. K. Madsen, and R. E. Slusher, "Optical delay lines based on optical filters," IEEE J. Quantum Electron. **37**, 525–532 (2001).
35. C. K. Madsen, G. Lenz, A. J. Bruce, M. A. Cappuzzo, L. T. Gomez, and R. E. Scotti, "Integrated all-pass filters for tunable dispersion and dispersion slope compensation," IEEE Photon. Technol. Lett. **11**, 1623–1625 (1999).
36. K. Djordjev, S. Choi, and P. D. Dapkus, "Microdisk tunable resonant filters and switches," IEEE Photon. Technol. Lett. **14**, 828–830 (2002).
37. J. E. Heebner and R. W. Boyd, "Slow and fast light in resonator-coupled waveguides," J. Mod. Opt. **49**, 2629–2636 (2002).
38. M. Notomi, K. Yamada, A. Shinya, J. Takahashi, C. Takahashi, and I. Yokohama, "Extremely large group-velocity dispersion of line-defect waveguides in photonic crystal slabs," Phys. Rev. Lett. **87**, 253902 (2001).
39. G. Lenz, B. J. Eggleton, C. R. Giles, C. K. Madsen, and R. E. Slusher, "Dispersive properties of optical filters for WDM Systems," IEEE J. Quantum Electron. **34**, 1390–1402 (1998).
40. S. L. McCall, A. F. J. Levi, R. E. Slusher, S. J. Pearton, and R. A. Logan, "Whispering-gallery mode microdisk lasers," Appl. Phys. Lett. **60**, 289–291 (1992).
41. Y. Yamamoto and R. E. Slusher, "Optical processes in microcavities," Phys. Today **46**(6), 66–74 (1993).
42. S. M. Spillane, T. J. Kippenberg, and K. J. Vahala, "Ultralow-threshold Raman laser using a spherical dielectric microcavity," Nature **415**, 621–623 (2002).
43. J. Popp, M. H. Fields, and R. K. Chang, "Q-switching by saturable absorption in microdroplets: elastic scattering and laser emission," Opt. Lett. **22**, 1296–1298 (1997).
44. F. C. Blom, D. R. van Dijk, H. J. Hoekstra, A. Driessen, and Th. J. A. Popma, "Experimental study of integrated-optics microcavity resonators: toward an all-optical switching device," Appl. Phys. Lett. **71**, 747–749 (1997).
45. V. Van, T. A. Ibrahim, K. Ritter, P. P. Absil, F. G. Johnson, R. Grover, J. Goldhar, and P.-T. Ho, "All-optical nonlinear switching in GaAs–AlGaAs microring resonators," IEEE Photon. Technol. Lett. **14**, 74–77 (2002).
46. T. A. Ibrahim, V. Van, and P.-T. Ho, "All-optical time-division demultiplexing and spatial pulse routing with a GaAs/AlGaAs microring resonator," Opt. Lett. **27**, 803–805 (2002).
47. J. E. Heebner, N. N. Lepeshkin, A. Schweinsberg, G. W. Wicks, R. W. Boyd, R. Grover, and P.-T. Ho, "Enhanced linear and nonlinear optical phase response of AlGaAs microring resonators," Opt. Lett. **29**, 769–771 (2004).
48. P. Chak, J. E. Sipe, and S. Pereira, "Depositing light in a photonic stop gap by use of Kerr nonlinear microresonators," Opt. Lett. **28**, 1966–1968 (2003).
49. S. Pereira, P. Chak, and J. E. Sipe, "Gap-soliton switching in short microresonator structures," J. Opt. Soc. Am. B **19**, 2191–2202 (2002).
50. S. Blair, "Nonlinear sensitivity enhancement with one-dimensional photonic bandgap microcavity arrays," Opt. Lett. **27**, 613–615 (2002).
51. M. Soljacic, S. G. Johnson, S. Fan, M. Ibanescu, E. Ippen, and J. D. Joannopoulos, "Photonic-crystal slow-light enhancement of nonlinear phase sensitivity," J. Opt. Soc. Am. B **19**, 2052–2059 (2002).
52. P. Absil, J. V. Hryniewicz, B. E. Little, P. S. Cho, R. A. Wilson, L. G. Jonekis, and P.-T. Ho, "Wavelength conversion in GaAs micro-ring resonators," Opt. Lett. **25**, 554–556 (2000).
53. S. T. Ho, C. E. Soccolich, M. N. Islam, W. S. Hobson, A. F. J. Levi, and R. E. Slusher, "Large nonlinear phase shifts in low-loss AlGaAs waveguides near half-gap," Appl. Phys. Lett. **59**, 2558–2560 (1991).
54. G. I. Stegeman, A. Villeneuve, J. Kang, J. S. Aitchison, C. N. Ironside, K. Al-Hemyari, C. C. Yang, C. H. Lin, H. H. Lin, G. T. Kennedy, R. S. Grant, and W. Sibbett, "AlGaAs below the half-gap: the silicon of nonlinear optical materials," Int. J. Nonlinear Opt. Phys. **3**, 347–371 (1994).
55. G. Lenz, J. Zimmermann, T. Katsufuji, M. E. Lines, H. Y. Hwang, S. Spalter, R. E. Slusher, S.-W. Cheong, J. S. Sanghera, and I. D. Aggarwal, "Large Kerr effect in bulk Se-based chalcogenide glasses," Opt. Lett. **25**, 254–256 (2000).
56. S. Spalter, H. Y. Wang, J. Zimmermann, G. Lenz, T. Katsufuji, S.-W. Cheong, and R. E. Slusher, "Strong self-phase modulation in planar chalcogenide glass waveguides," Opt. Lett. **27**, 363–365 (2002).
57. J. M. Harbold, F. O. Ilday, F. W. Wise, J. S. Sanghera, V. Q. Nguyen, L. B. Shaw, and I. D. Aggarwal, "Highly nonlinear As–S–Se glasses for all-optical switching," Opt. Lett. **27**, 119–121 (2002).
58. P. Chak, J. E. Sipe, and S. Pereira, "Lorentzian model for nonlinear switching in a microresonator structure," Opt. Commun. **213**, 163–171 (2002).
59. S. Pereira, P. Chak, and J. E. Sipe, "All-optical AND gate by use of a Kerr nonlinear microresonator structure," Opt. Lett. **28**, 444–446 (2003).
60. B. E. Little and S. T. Chu, "Estimating surface roughness loss and output coupling in microdisk resonators," Opt. Lett. **21**, 1390–1392 (1996).
61. V. B. Braginsky and V. S. Ilchenko, "Properties of optical dielectric microresonators," Sov. Phys. Dokl. **32**, 306–307 (1987).
62. S. Arnold, C. T. Liu, W. B. Whitten, and J. M. Ramsey, "Room-temperature microparticle-based persistent spectral hole burning memory," Opt. Lett. **16**, 420–422 (1991).
63. N. Dubreuil, J. C. Knight, D. K. Leventhal, V. Sandoghdar, J. Hare, and V. Lefevre, "Eroded monomode optical fiber for whispering-gallery mode excitation in fused-silica microspheres," Opt. Lett. **20**, 813–815 (1995).
64. M. L. Gorodetsky, A. A. Savchenkov, and V. S. Ilchenko, "Ultimate *Q* of optical microsphere resonators," Opt. Lett. **21**, 453–455 (1996).
65. D. W. Vernooy, V. S. Ilchenko, H. Mabuchi, E. W. Streed, and H. J. Kimble, "High-*Q* measurements of fused-silica microspheres in the near infrared," Opt. Lett. **23**, 247–249 (1998).
66. J.-P. Laine, B. E. Little, and H. A. Haus, "Etch-eroded fiber coupler for whispering-gallery-mode excitation in high-*Q* silica microspheres," IEEE Photon. Technol. Lett. **11**, 1429–1430 (1999).
67. M. Cai, O. Painter, and K. Vahala, "Observation of critical coupling in a fiber taper to a silica-microsphere whispering-galley mode system," Phys. Rev. Lett. **85**, 74–77 (2000).
68. S. Blair, J. E. Heebner, and R. W. Boyd, "Beyond the absorption-limited nonlinear phase shift with microring resonators," Opt. Lett. **27**, 357–359 (2002).

69. J. P. Zhang, D. Y. Chu, S. L. Wu, S. T. Ho, W. G. Bi, C. W. Tu, and R. C. Tiberio, "Photonic-wire laser," Phys. Rev. Lett. **75**, 2678–2681 (1995).
70. S. Fan, P. R. Villeneuve, J. D. Joannopoulos, and H. A. Haus, "Channel drop filters in photonic crystals," Opt. Express **3**(7), 4–11 (1998).
71. M. D. Rahn, A. M. Fox, M. S. Skolnick, and T. F. Krauss, "Propagation of ultrashort nonlinear pulses through two-dimensional AlGaAs high-contrast photonic crystal waveguides," J. Opt. Soc. Am. B **19**, 716–721 (2002).
72. S. Mingaleev and Y. Kivshar, "Nonlinear transmission and light localization in photonic-crystal waveguides," J. Opt. Soc. Am. B **19**, 2241–2249 (2002).
73. C. V. Bennett and B. H. Kolner, "Upconversion time microscope demonstrating 103× magnification of femtosecond waveforms," Opt. Lett. **24**, 783–785 (1999).